JACS
JOURNAL OF THE AMERICAN CHEMICAL SOCIETY
Article
pubs.acs.org/JACS

Structural Principles of RNA Catalysis in a 2′−5′ Lariat-Forming Ribozyme

Teresa Carlomagno,*[,‡] Irene Amata,[‡] Luca Codutti,[‡] Melanie Falb,[‡] Jörg Fohrer,[§] Pawel Masiewicz,[‡] and Bernd Simon[‡]

[‡]Structural and Computational Biology Unit, EMBL, Meyerhofstraße 1, D-69117 Heidelberg, Germany
[§]Max Planck Institute for Biophysical Chemistry, Am Faßberg 11, D-37077 Göttingen, Germany

Supporting Information

ABSTRACT: RNA-catalyzed lariat formation is present in both eukaryotes and prokaryotes. To date we lack structural insights into the catalytic mechanism of lariat-forming ribozymes. Here, we study an artificial 2′−5′ AG1 lariat-forming ribozyme that shares the sequence specificity of lariat formation with the pre-mRNA splicing reaction. Using NMR, we solve the structure of the inactive state of the ribozyme in the absence of magnesium. The reaction center 5′-guanosine appears to be part of a helix with an exceptionally widened major groove, while the lariat-forming A48 is looped out at the apex of a pseudoknot. The model of the active state built by mutational analysis, molecular modeling, and small-angle X-ray scattering suggests that A48 is recognized by a conserved adenosine, juxtaposed to the 5′-guanosine in one base-pair step distance, while the G1-N7 coordinates a magnesium ion essential for the activation of the nucleophile. Our findings offer implications for lariat formation in RNA enzymes including the mechanism of the recognition of the branch-site adenosine.

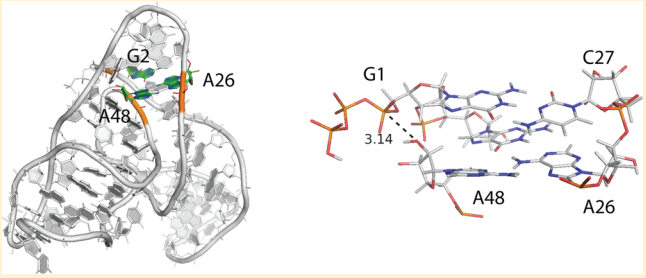

INTRODUCTION

Introns are removed from precursor pre-mRNAs in eukaryotic cells during mRNA maturation. The process, called splicing, is highly regulated and critical to gene expression. The machinery responsible for intron excision and exon ligation is a large ribonucleoprotein complex, the spliceosome.[1] In the spliceosome, splicing proceeds through two transesterification reactions: in the first step, the 2′-hydroxyl of an adenosine within the intron attacks the 5′ exon−intron junction, resulting in the release of the 5′ exon and formation of a lariat RNA; in the second step, the 3′ end hydroxyl of the released 5′ exon attacks the intron−3′ exon junction, completing the splicing and releasing a lariat RNA intron. The lariat form contains an unusual triply linked (2′, 3′, and 5′) nucleotide (nt).[1]

Splicing via formation of lariat RNA is not exclusive to eukaryotes. Bacteria, organelles, and viruses contain self-splicing group II introns that catalyze their own excision from precursor mRNA through two transesterification reactions resembling the two steps of eukaryotic pre-mRNA splicing.[2]

The observation that both group II introns and nuclear introns are processed through the formation of lariat RNA has led to the hypothesis that spliceosomal catalysis might be supported primarily by the spliceosomal (sn) RNA.[3−6] Despite the importance of the intron splicing process via lariat formation, an atomistic picture of the catalytic mechanisms is still lacking. An atomic-resolution structure of the catalytic core of the spliceosome is unavailable, and the structural studies of spliceosomal sub-complexes published in the past decade (reviewed in ref 1) fail to provide such insight.

The recently reported crystallographic structure of the group II intron from the alkaliphile *Oceanobacillus iheyensis*[8] has revealed a wealth of information on the tertiary structure and principles of RNA−RNA recognition around the active site of this ribozyme; however, the catalytic core of the intron remained disordered in the structure. In a more recent study, the structure of the 5′ splice site could be detected in a crystal of the same group II intron in the precatalytic state at 3.65 Å resolution.[9]

In this work we use a combined approach consisting of complementary biophysical and biochemical techniques to study the structure of a model 2′−5′ AG1 lariat-forming ribozyme. This ribozyme was identified by an in vitro selection from a library of 2×10^{14} different sequences based on the sequence of the U6 snRNA[7,10] (Figure 1). It contains 59 nucleotides including the conserved U6 ACAGAGA box sequence that is essential for catalytic activity in the spliceosome. Moreover the branch formation has the same sequence specificity as in pre-mRNA, including the attack of the 5′-phosphate of a guanosine by the 2′-OH group of an internal adenosine with formation of a 2′−5′ branched lariat. In the case of the ribozyme, the guanosine is at the 5′ terminus and the reaction proceeds with diphosphate release.

Received: December 10, 2012
Published: March 8, 2013

   dx.doi.org/10.1021/ja311868t | *J. Am. Chem. Soc.* 2013, 135, 4403−4411

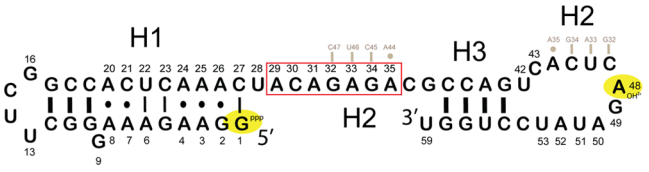

Figure 1. Primary and secondary structure of the 2′−5′ AG1 lariat-forming ribozyme. Bold lines indicate Watson−Crick (WC) base pairs previously proposed on the basis of covariation experiments[7] and here verified by NMR; thin lines and dots indicate respectively WC and non-canonical base-pairs found by NMR analysis. The stretch 32−35 is base-paired with the stretch 44−47 (in gray), forming a pseudoknot through nucleotides 32−58. The G1 and the A48 are involved in the transesterification reaction leading to lariat RNA (yellow shadows). The conserved ACAGAGA box is marked in red. The three helical stretches are marked as H1, H2, and H3.

With a combination of NMR, mutational analysis, and molecular modeling, we uncover the structure of the 2′−5′ AG1 lariat-forming ribozyme in the inactive state and provide a model of the catalytically active form. Our results suggest the recognition of the branch-site adenosine by a N6,N7 base pair with a conserved adenosine juxtaposed to the 5′-guanosine in one base-pair step distance. The 2′-OH of the branch-point adenosine may be activated by a magnesium ion coordinated between the α-phosphate and the N7 of the 5′-guanosine. The compact fold of the active state of the ribozyme is likely stabilized by magnesium ions bridging phosphate groups of nearby backbone segments, in agreement with previous data from phosphorothioate interference experiments.[7]

This first atomic view of the catalytic site of a lariat-forming ribozyme sets the basis for understanding catalysis in this important class of enzymes and offers new testable models for the mechanism of group II introns and the spliceosome.

MATERIALS AND METHODS

Sample Preparation and Activity Tests. The RNA was prepared by in vitro transcription using T7 polymerase produced in house. For structural studies a 3′-extended construct was produced and cut in trans by a hammerhead ribozyme to obtain a well-defined 3′ end. Formation of the lariat for the wild-type and mutant RNAs was monitored by gel electrophoresis after overnight incubation of the RNA with 25 mM [Mg^{2+}] at 30 °C and pH 7.6. Under these conditions the wild-type RNA produces ∼60% of lariat RNA. The A39-N7-deaza and N6-Me ribozymes of sequence 5′-GGAGCGCCA-CUGGAAAACUACAGAGACGCCAGUCACUCAGAUAUCCUGG-3′ were purchased by IBA and were tested for activity in combination with the substrate 5′pppGGAAAUGCCCAAGCGCUC-3′, as described in ref 7.

NMR Analysis. The resonance assignment of the 2′−5′ AG1 branch-forming ribozyme in the absence of Mg^{2+} was based on the following experiments: 2D $^{13}C/^{15}N$-edited HSQCs, 2D HNN-COSY,[11,12] 2D imino NOESY, 3D HsCNb/HbCNb,[13] 3D HCCH−COSY-TOCSY,[14] 3D ^{13}C-edited/^{13}C-filtered NOESY and 3D ^{13}C-edited/^{12}C-filtered NOESY[15] acquired on the following selectively labeled samples: (1) $^{13}C,^{15}N$ A-labeled RNA; (2) $^{13}C,^{15}N$ G-labeled RNA; (3) $^{13}C,^{15}N$ C-labeled RNA; (4) $^{13}C,^{15}N$ U-labeled RNA; and (5) $^{13}C,^{15}N$ AU-labeled RNA. All experiments were acquired at 800 or 900 MHz Bruker spectrometers equipped with cryoprobes. NOEs were measured in 3D ^{13}C-edited/^{13}C-filtered NOESY, 3D ^{13}C-edited/^{12}C-filtered NOESY,[15] and 2D imino NOESY spectra. All NMR experiments were acquired at pH 6.6 in 20 mM sodium phosphate buffer at 298 K. Samples had concentrations varying between 0.1 and 0.5 mM. After purification, the RNA was extensively dialyzed against 1 M NaCl, to remove residual bound magnesium, and subsequently slowly dialyzed in the final buffer, which did not contain any NaCl. Addition of NaCl did not change the NMR signals. The chemical shifts have been deposited at the Biological Magnetic Resonance Bank (BMRB) with code rcsb103224.

Structure Calculations. Structures were calculated using the Aria 1.2/CNS 1.1 setup[16,17] (details in the Supporting Information). A total of 1234 unambiguous and 105 ambiguous NOE distances were categorized as weak (2.0−5.5 Å), medium (2.5−4.0 Å), or strong (1.8−3.0 Å). The ribose conformation of nt's 1−12, 17−27, 32−34, 39−41, 45−47, and 55−57 of helix H1, H2, or H3 was restrained to the C3′-endo range, as indicated by the analysis of the chemical shifts of the C1′, C4′, and C5′ carbons.[18] The dihedral angles α, β, ε, and ζ were restrained to A-form helix ranges 300° ± 30°, 180° ± 30°, −135° ± 30°, and 300° ± 30°, respectively, for nt's 5, 10−12, 17−19, 23, 32−34, 38−41, 45, 46, and 55−57, involved in canonical WC base pairs, and loosely to the allowed ranges 180° ± 150°, 180° ± 110°, −125° ± 75°, and 180° ± 150°, respectively, for all other nucleotides. The dihedral angle γ was restrained to the gauche+ range for nucleotides involved in canonical base pairs only. The χ angles of 39 nucleotides were restricted to the anti conformation on the basis of the intensities of the intranucleotide H8−H1′ (Pu) and H6/H5−H1′ (Py) NOEs. The structure of the ribozyme in its inactive state has been deposited in the Protein Data Bank (PDB) with code 2m58.

Calculation of the Model for the Active State. The model of the active form was calculated in a similar manner as the structure of the inactive form. In addition to the NMR derived restraints defining the structures of helix H1 and of the 3′-terminal pseudoknot, hydrogen bonds restraints were added between A48-N6 and N7 and A26-N7 and N6, respectively; co-planarity was imposed for the base rings of A26 and A48. A distance restraint of 2.5 ± 0.5 Å was imposed between the G1-Pα and the A48-2′-O. NOEs stemming from A31 and G49 were eliminated to allow for rearrangements of the relative position of the 5′-terminal helix and the 3′-terminal pseudoknot in the active state. Weak restraints were imposed between the bases of A3/A4 and the phosphates of A48/C47.

Positioning of the Mg^{2+} Ions. Molecular dynamics runs of the 2′−5′ AG1 lariat-forming ribozyme were prepared using the AmberTools 11.0 suite and run using AMBER 11.[19] The system in analysis consists of a molecule of ribozyme whose charges are counterbalanced by K^+ ions in explicit TIP3P water.[20] First, K^+ ions were allowed diffusing in the RNA structure of the active form model during 1.0 ns of molecular dynamics (MD) at constant pressure (1 atm) and temperature (300 K), using a Langevin thermostat. From the K^+ ions with a residence time at the RNA molecule >50%, 8 ions occupying conserved sites in all runs were selected, corresponding to a final concentration of ca. 30 mM, and changed to Mg^{2+} ions for subsequent MD. The equilibration with Mg^{2+} was divided in 14 steps, for a total amount of 0.62 ns, gradually releasing a restraint mask from heavy atoms from 10 to 0.001 kcal mol^{-1} $Å^{-2}$.[21] A distance restraint with average value of 3.0 Å was imposed between G1-Pα and A48-2′-O with force of 5 kcal mol^{-1} $Å^{-2}$ during the simulation; furthermore, co-planarity (15 kcal mol^{-1} $Å^{-2}$) and distance restraints (5 kcal mol^{-1} $Å^{-2}$) were imposed between bases A48 and A26. Details of the protocol are in the Supporting Information.

Small-Angle X-ray Scattering (SAXS) Data. SAXS experiments were recorded on the A48-2′-OCH_3 2′−5′ AG1 lariat-forming ribozyme. Samples were titrated with increasing amounts of $MgCl_2$ at RNA concentrations of 0.5 and 1 mg/mL. Data were collected at the ESRF BioSAXS beamline ID14EH3.[22] Standard data collection was used, employing an automated robot, mounting the samples to a capillary, and collection of 10 frames of 10 s duration in flow-through mode, using a total of 30 μL of sample. The 10 frames were added automatically by the data collection software. The buffer scattering was measured before and after each sample and subtracted using the program PRIMUS.[23] Radius of gyration was obtained by extrapolating the values at 0.5 and 1 mg/mL to zero RNA concentration.

RESULTS

NMR Analysis of the 2′−5′ Lariat-Forming Ribozyme. To discover the fold of the 2′−5′ AG1 lariat-forming ribozyme

dx.doi.org/10.1021/ja311868t | J. Am. Chem. Soc. 2013, 135, 4403−4411

in its inactive state (PDB code 2m58), we determined the structure of this 59mer RNA (Figure 1) in solution in the absence of Mg^{2+} ions by NMR. The $^{1}H-^{13}C$ correlation of the $^{13}C/^{15}N$ uniformly labeled RNA, as well as those of $^{13}C/^{15}N$ selective U-, A-, C-, and G-labeled RNAs are heavily overlapped in both the base and the ribose regions (Figure S1). In addition, more than the 59 expected resonances are visible in the H8,H6/C8,C6 and H1′/C1′ correlations. Analysis of ^{13}C-edited NOESY spectra indicates that nt's 30−59 are present in two conformations, which slowly exchange with each other (Figure S2). Resonances belonging to the less populated conformation (∼35%) do not show internucleotide NOEs, indicating that the ribozyme lacks a defined structure from nt's 30 to 59 in this conformation. The structure that we present here refers to the major, completely folded conformation.

The resonance assignment and the analysis of the NOESY spectra for this 59mer RNA offered several challenges, including extreme spectral overlap, the presence of 89 resonance sets, instead of 59, and the inhomogeneous intensity of nucleotide resonances belonging to different RNA regions. To cope with these challenges, we collected data sets for five selectively labeled samples using mostly ^{13}C-edited, ^{12}C-filtered/^{13}C-filtered experiments (see Materials and Methods and Supporting Information).[15] Moreover, to confirm the assignment of ambiguous regions, we synthesized several single- or double-nucleotide mutant RNAs (Figure 2). Finally, more than 95% of the base resonances and 82% of the ribose resonances could be assigned unambiguously.

^{13}C-edited, ^{12}C-filtered, and ^{13}C-edited, ^{13}C-filtered NOESY spectra[15] on $^{13}C/^{15}N$ selective AU-, U-, A-, C-, and G-labeled RNAs resulted in 1339 assigned NOEs for structure calculation, corresponding to an average of 23 restraints per residue. Covariation experiments had previously identified base-paired nucleotides,[7] indicated with bold lines in Figure 1. We confirmed the presence of these base pairs by inspection of the imino proton region of ^{15}N-HSQC and HNN-COSY[12] 2D spectra.

A continuous network of strong H8/H6(i)-H2′(i−1) NOEs, accompanied by medium H8/H6(i)-H1′(i−1) NOEs and weak H8/H6(i)-H8/H6(i−1), suggested the extension of helix H1 from nt 1 to nt 27, over five non-canonical base pairs (2·26, 3·25, 4·24, 7·21, and 8·20) and three canonical base pairs (1−27, 5−23 and 6−22) (Figure 1).

To confirm the presence of an extended helix H1, we performed mutational analysis (Figure 2), which confirmed the existence of base pairs 5−23, 6−22, 7·21, and 1−27 by either single-point or compensatory double-point mutations (Figure 2). In addition, the mutational analysis showed that the non-canonical base pairs 2·26, 3·25, and 4·24 can be substituted by nucleotide combinations compatible with Watson−Crick (WC) base pairs (U2-A26, A3-U25, and A4-U24), as long as the identity of nt's 3, 4, and 26 is preserved. G9 can be removed without any impact on catalytic activity (Figure 2) and is therefore not part of the helix, as already predicted by the NOE pattern in the A8-G10 segment. The revised secondary structure for the stretch 1−27 of the 2′−5′ AG1 lariat-forming ribozyme is depicted in Figure 1. Prior to calculating the structure of the RNA from NOE data, the topology of the non-canonical base pairs 8·20, 7·21, 4·24, 3·25, and 2·26 was derived as described in the Supporting Information. To summarize, cis WC-WC topology[24] was found for all these base pairs (see hydrogen-bonding patterns in Table S1). The cis WC-WC base pairs can be well integrated in the helical geometry suggested

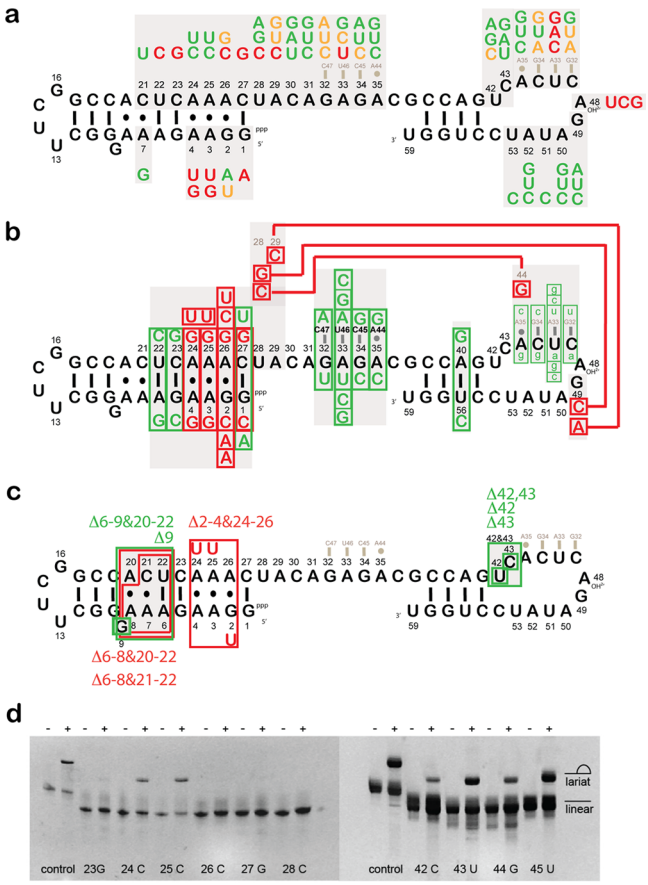

Figure 2. Mutational analysis of the 2′−5′ AG branch-forming ribozyme. (a) Single-nucleotide mutants. Red, yellow and green colors indicate mutants blocking (no lariat), reducing (<20%). and not affecting (20−70%) the lariat formation, respectively. (b) Double-nucleotide mutants. The color code is as in panel a. (c) Deletion and three-nucleotide mutants. The color code is as in panel a. The boxed residues were deleted in each deletion variant, as indicated in the figure. (d) Example of mutational analysis for the stretch 23−28 and 42−45. (−) and (+) indicate the absence and the presence of 25 mM Mg^{2+}. Formation of the lariat was monitored after overnight incubation at 30 °C. For the control, a longer RNA, which was extended at 3′-end by 8 nucleotides, was used. This RNA produces the same fraction of lariat as the 59mer construct.

by the NOEs, and are fully consistent with our mutational data (Figure 2).

In the stretch containing nt's 28−59, the analysis of the imino proton region of the $^{15}N-^{1}H$ correlation confirmed the presence of the canonical base pairs encompassing nt 38−41 and 55−58, which had been inferred by covariation experiments.[7] In addition, the 3D NOESY spectra revealed a continuous network of strong H8/H6(i)−H2′(i−1) NOEs, accompanied by medium H8/H6(i)−H1′(i−1) NOEs and weak H8/H6(i)−H8/H6(i−1) in the stretch 44−47 and, to a lesser extent, in the stretch 32−35. Besides, NOEs were present between C47 and A50, between U46 and both U51 and A52, and between A35 and U53. The NOEs are indicative of a pseudoknot structure, with two short (4 base pairs) helical segments (H2 and H3 in Figure 1) and the stretch 50−53 contacting the minor groove of helix H2. The base pairing between stretches 44−47 and 32−35 is critical to the structure and was therefore confirmed by compensatory mutations (Figure 2). The six catalytically impaired mutants G32U, A33U,

dx.doi.org/10.1021/ja311868t | J. Am. Chem. Soc. 2013, 135, 4403−4411

A33C, and G34C can be rescued by complementary mutations C47A, U46A, U46G, and C45G, respectively, supporting the notion that the stretches 44−47 and 32−35 are mutually base-paired (Figure 1). The non-canonical A35·A44 base pair was found to be in the trans WC-Hoogsteen topology, as described in the Table S1.

Structure of the 2′−5′ AG1 Lariat-Forming Ribozyme in the Absence of Magnesium Ions. The structure calculation (details in Materials and Methods and Supporting Information; statistics in Table 1) converged to a well-defined

Table 1. Structure Statistics (10 Structures of 200 Calculated, PDB code 2m58)

	in vacuum	water refined
Distance Restraints		
total unambiguous NOEs	1234	
inter-residue	569	
sequential ($\|i-j\|=1$)	631	
long-range ($\|i-j\|>2$)	34	
total ambiguous NOEs	105	
dihedral angle restraints	383	
hydrogen bonds	20	
Structure Statistics		
Deviations from Idealized Geometry		
bond lengths (Å)	0.0060 ± 0.0001	0.0042 ± 0.0001
bond angles (deg)	0.74 ± 0.01	0.96 ± 0.02
impropers (deg)	0.50 ± 0.01	0.70 ± 0.02
Violations (Mean and SD)		
distance restraints rmsd (Å)	0.08 ± 0.01	0.12 ± 0.01
distance restraint violations >0.5 Å	0.4 ± 0.7	10.1 ± 1.8
dihedral angle restraints rmsd (deg)	1.48 ± 0.09	1.65 ± 0.12
dihedral angle violations >5°	4.7 ± 1.3	5.7 ± 1.5
Coordinate Precision (Å)		
backbone (1−27)	1.22 ± 0.30	1.34 ± 0.31
heavy atoms (1−27)	1.15 ± 0.26	1.28 ± 0.26
backbone (32−58)	1.34 ± 0.48	1.38 ± 0.31
heavy atoms (32−58)	1.75 ± 0.50	1.86 ± 0.39

conformation for stretches 1−27 (excluding G9 and the 5′-triphosphate, heavy atom root-mean-square deviation, rmsd = 0.83 Å) and helices H2, H3 (heavy atom rmsd = 0.97 Å) (Figure S3).

The 5′-terminal stretch folds into a 12 base pair long helix closed at one apex by the UUCG tetraloop. This helix contains several non-canonical base pairs (see above), and thus its overall conformation significantly deviates from ideal A-form RNA (Figure 3b, Table S2). The inclination angles of the base pairs with respect to the helix axis are lower than for A-form helices and approximate those for A′-RNA. The inter base pair rise values (average value 3.1 Å) are between those of A′-RNA and B-DNA. This unwinding of the helix is caused by a continuous stacking of six purine bases on one strand and three purine bases on the other strand (Figure 3c). The major groove is substantially widened (ca. 11 Å) with respect to that of A-RNA (3.8 Å) or even A′-RNA (8.0 Å) and resembles that of B-DNA (11.4 Å) (Table S2). Such opening of the major groove around base pairs G2·A26, A3·A25, A4·A24, and G5·C23 makes this region of the AG1 lariat-forming RNA unusually accessible to interactions with ligands or with other structural elements of the same RNA. Consistently, our mutational analysis of the upper part of the 5′-terminal helix of the RNA

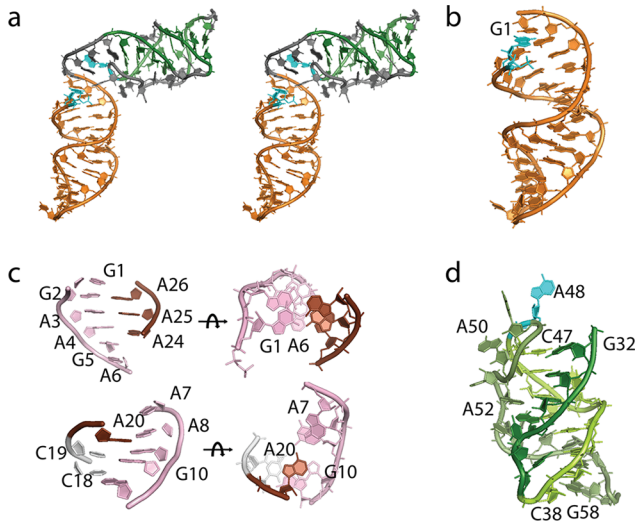

Figure 3. Structure of the 2′−5′ AG1 branch-forming ribozyme. (a) The 2′−5′ lariat-forming ribozyme folds into a 5′-terminal helix comprising nt's 1−27 (orange) and a 3′-terminal pseudoknot comprising nt's 32−59 (green and gray). The pseudoknot structure brings A48 (cyan) in proximity of G1 (cyan). The relative position of the 5′-terminal helix and the 3′-terminal pseudoknot is variable in the absence of Mg^{2+}. For clarity only one structure is shown in cross-eye stereoview. A superimposition of all structures of the NMR ensemble can be found in Figure S3. (b) 5′-terminal helix showing the wide and shallow major groove at the 5′ end of the helix. (c) Stacking of purine residues in the 5′-terminal helix. Upper panels: Stacking of a six purine stretch on one strand (pale pink) and a three purine stretch on the opposite strand (aubergine) in the first six base pairs of the 5′-terminal domain. Lower panels: Stacking of two and three purine stretches in the apical part of the 5′-terminal helix (in pale pink and aubergine). The stack of three purines contains a cross-strand stacking between G10 (pale pink) and A20 (aubergine). Pyrimidines are shown in white. For clarity, the bonds between the riboses and the bases have been omitted in the left half. (d) 3′-terminal pseudoknot. Strand 32−37 is in dark green, strand 38−47 in lime and strand 49−59 in mud green; the A48 is in cyan. Two short helical segments are formed by nt's 32−35, which base-pair with the stretch 47−44, and by nt's 38−41, which base-pair with nt's 58−55. The stretch 50−53 contacts the minor groove of the first helical segment.

indicates that the widening of the major groove in this region is relevant for the catalytic function of the RNA. A24U or A25U single mutants, which are compatible with canonical base pairing at single sites, are catalytically competent, suggesting that one WC base pair might be tolerated without loss of function. On the other hand, A24U/A25U double mutants or the G2U/A24U/A25U triple mutant lack activity; this is compatible with the notion that two consecutive WC base pairs would bring the helix closer to A-form, with a deeper and narrower major groove; this structure is evidently unable to support catalysis (Figure 2).

The grooves gradually narrow toward the lower part of the helical segment. Next to the tetraloop (Figure 3b, Table S2), the major groove width is within 7−8 Å close to the value for A′-RNA. This part of the helix displays two stacks of two and three purine bases each, including a cross-strand stack between A20 and G10 (Figure 3c).

The 3′-terminal stretch (nt's 32−59) folds into a pseudoknot structure (Figure 3d). Two short helices comprising nt's 32−35 and 44−47 (helix H2) and nt's 38−41 and 55−58 (helix H3) stack upon each other. The nt's 42 and 43 are bulged out. The

dx.doi.org/10.1021/ja311868t | J. Am. Chem. Soc. 2013, 135, 4403−4411

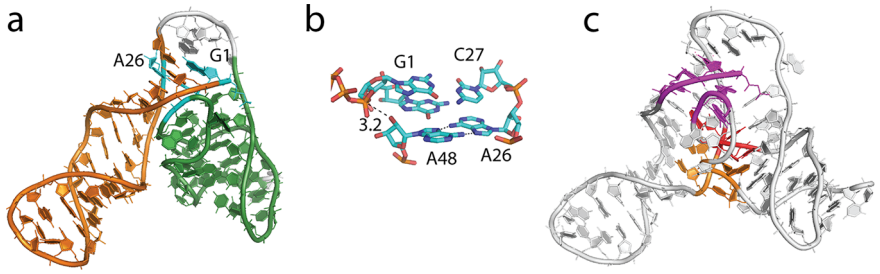

Figure 4. Possible model of the compact fold of the active state of the 2′−5′ AG1 lariat-forming ribozyme. (a) In the presence of Mg^{2+} the ribozyme can assume a compact fold, stabilized by interactions between residues of the 3′-terminal pseudoknot (green) and the major groove of the H1 helix (orange). A48, G1 and A26 are shown in cyan. (b) A48 can be recognized by A26. In the model A48 uses its Hoogsteen face to contact the Hoogsteen face of A26 forming two N6−N7 hydrogen bonds. The 2′-OH of A48 is located in proximity of the α-phosphate of G1 and can initiate the transesterification reaction. Distances are in Å. (c) Regions of the backbone in close proximity to each other are colored: magenta, G1-A3 with A48-G49; orange, U22−C23 with A52-U53; red, A24 with C45−U46. These regions correspond to those where phosphorothioate interference experiments[7] suggested binding of Mg^{2+}.

Δ42,43 mutant is catalytically active, confirming that these two nucleotides are not part of any essential structural element. The existence of helix H2 was confirmed by mutational analysis: The inactive mutant RNA A33U and the weakly active mutants G32U and G34C could be rescued by compensatory mutations U46A, C47A, and C45G (Figure 2). The stretch A50-U53 contacts the minor groove of helix H2, with A52 positioned favorably to form a base triple with the sugar edge face of G34. The pseudoknot structure induces a sharp kink in the RNA backbone after C47; as a result, nt's 48 and 49 are looped out. A48 comes close to the 5′ terminus of helix H1 and is available for recognition via tertiary interactions with structural elements within the helix (Figure 3a).

The stretch 28−31, connecting the 5′ helix H1 and the 3′-terminal 32−58 pseudoknot is not well defined. In most structures U28 stacks on C27 of helix H1, while A31 stacks on G32 at the start of the 3′-terminal pseudoknot. The NOEs of A29 and C30 are compatible with more than one conformation, which suggests that in the ground state the relative orientation of helix H1 and the 3′-terminal pseudoknot is not fixed but samples multiple conformations in a dynamic equilibrium (Figure S3). However, a weak NOE between A29-H2 and G49-H1′ and several NOEs between C47 and G49 confirm the pseudoknot structure, the extrusion of A48 and the proximity of the A48-G49 nucleotides with the 3′ end of helix H1.

Structural Model of the Active Form of the 2′−5′ Lariat-Forming Ribozyme. The 2′−5′ lariat-forming ribozyme performs catalysis in the presence of magnesium. In theory, the structure of the active form of the ribozyme could be determined by trapping the active state via adding magnesium to a catalytically incompetent form of the RNA (for example, with a 2′-deoxyadenosine at position 48). Unfortunately, the synthesis of such a modified RNA with the many $^{13}C/^{15}N$ labeling schemes necessary for structural investigation by NMR, is impractical. In this study, we choose to build a model of the active form of the ribozyme on the basis of its structure in the inactive form (in the absence of magnesium), the enzymatic activity of the mutants and molecular modeling.

The mutant analysis showed that the nature of four bases, A3, A4, A26, and A48 is essential to sustain catalytic activity. In the wild-type ribozyme, A3 and A4 form non-canonical base pairs with A25 and A24, respectively. The single mutations A24U and A25U are tolerated, while the double mutant A24U/A25U is inactive. These data underline the importance of a widened major groove around A3 and A4 and suggest that these nucleotides are involved in the tertiary recognition of other RNA structural elements. A26 is also crucial to catalysis; furthermore, the reduced activity of the G2U mutant underlines the relevance of a widened major groove at this position. All in all, these data point at a specific recognition of the base of A48 by either A3 or A4 or A26 or a combination thereof.

The terminal nucleotide carrying the reactive 5′-triphosphate must form a canonical base pair, as indicated by the loss of catalytic activity in the G1A mutant, which can be rescued by the complementary mutation C27U (Figure 2). This conclusion is supported by the loss of activity of the mutant Δ6−8/Δ20−22, where the base pair register in H1 is shifted by one nucleotide. Further deletion of the unpaired G9 in the Δ6−9/Δ20−22 mutant restores activity, indicating that the length of the 5′-terminal helix H1 is not essential and that the recognition of the catalytic center is confined to the 5′-terminal base pairs.

With this information in our hands we constructed a model for the active state of the 2′−5′ lariat-forming ribozyme (detailed protocol in Supporting Information). We argued that the two secondary structure elements present in the inactive state, the 5′-terminal helix H1 and the 3′-terminal pseudoknot, are rather rigid structures; however, they can likely move with respect to each other via the hinge region (around nt's 28−31). In the active state of the ribozyme the two secondary structure elements must come closer to each other in a way that the 2′-OH of the A48 ribose can reach to the 5′-phosphate of G1.

With this restraint in mind, the base of A48 can be recognized solely by A26. Trial structure calculations imposing proximity of any functional group of the base of A48 with either A3 and A4 showed that these configurations are incompatible with A48-2′-OH being close to the G1 phosphate. In contrast, if A48 is recognized by A26 with two A48-N7−A26-N6 and A48-N6−A26-N7 hydrogen bonds, the A48-2′-OH group comes in close proximity (~3.0 Å) to the G1 α-phosphate (Figure 4a,b). In this conformation, A48 forms a base triple with the A26 of the G2·A26 base pair. The phosphates of A48 and C47 contact the major groove of the 5′-terminal helix and come close to the exocyclic amino groups of A3 and A4. This favorable electrostatic interaction adds to the recognition of A48 and might explain the need for adenosines at positions 3 and 4.

To support the base triple formed by A48 with the A26 of the G2·A26 base pair, we performed lariat-formation assays

dx.doi.org/10.1021/ja311868t | J. Am. Chem. Soc. 2013, 135, 4403−4411

with ribozymes carrying modified A48. Both the A48-N7-deaza and the A48-N6-Me ribozymes were completely inactive, which strongly supports the involvement of the Hoogsteen face of A48 in the recognition of the branch-site adenosine.

The low-field shift of both the C3′ and the C4′ carbons of A48 in the inactive state (80.2 and 83.4 ppm, respectively), indicate that the ribose populates, to a large extent, the C2′-endo conformation. In addition, the low-field-shifted resonances of both the H2′ and H3′ protons (5.30 and 5.07 ppm, respectively) suggest that the base is in the syn conformation. The conformational preferences of the ribose of A48 in the ribozyme inactive state are similar to the conformation of our model of the active state, where the A48 ribose assumes a conformation close to C2′-endo. In addition, a small H1′−H8 NOE peak suggests that the syn conformation of the A48 base, observed in the model of the active state, is considerably populated also in the inactive state.

The stretch 28−31 as well as the stretch 49−53 do not form any base-specific tertiary contacts in our structural model of the active state. This is in agreement with the notion that any substitution at positions 49−53 is compatible with catalytic activity, as well as any substitution at positions 30 and 31.

Intriguingly, the U28C mutant does not support catalysis, despite the fact that this nucleotide is not involved in any sequence specific contacts in the structure.

We reasoned that the lack of activity of the U28C mutant could be determined by a particular structural feature of this mutant that impedes the recognition of A48, for example by formation of a base pair between U28 and G49. Indeed, the catalytically active mutant U28G can be turned into a catalytically incompetent mutant by the mutation G49C, while the single mutant G49C is active. This confirms that formation of a base pair between nt's 28 and 49 is detrimental for activity.

These observations suggest that the 28−31 stretch is flexible and this flexibility is essential for the function of the ribozyme, strongly supporting the notion that it functions as a hinge the 5′ and 3′ rigid structural motifs pivot on.

Interestingly, in the modeled compact active conformation, the backbone phosphates of A48-G49 are in close proximity to the backbone phosphates of G2-A4 and the G1 α-phosphate. In addition, the backbone of C45 and U46 approaches the backbone of A24 on the other strand of the 5′-terminal helix (Figure 4c), and the backbone of A52 and U53 comes close to the backbone of U22 and C23 (Figure 4c).

It is likely that such tertiary contacts require divalent cations to disperse the high density of negative charges on the close-by phosphate groups, and thus we predict that closing of the structure will be concomitant with the addition of divalent ions. To verify this and provide additional support for our active ribozyme model, we performed SAXS analysis of the A48-2′-OCH_3 2′−5′ AG1 ribozyme, which is catalytically incompetent due to methylation of the A48-2′-O position. The radius of gyration (R_g) that can be extracted from the first (linear) part of the scattering curve reports on the shape of the molecule.

Figure 5 shows the radius of gyration extracted from the SAXS curve of a 0.5 mg/mL solution of A48-2′-OCH_3 2′−5′ AG1 lariat-forming ribozyme in the presence of increasing concentrations of Mg^{2+} (0−13 mM). The R_g decreases from 3.1 to 2.1 nm, confirming the transition from the extended form in the inactive state with no Mg^{2+}, where the relative orientation of helix H1 and the 3′-terminal pseudoknot is poorly determined, to an overall more compact fold of the active state.

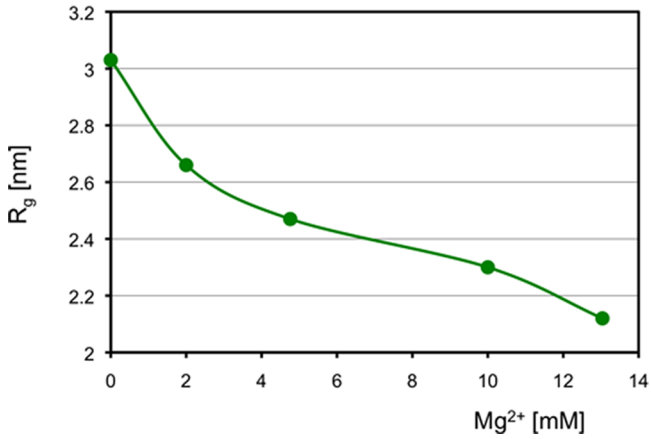

Figure 5. SAXS analysis of the ribozyme in the presence of Mg^{2+}. Radius of gyration (R_g, y-axis, in nm) extracted from the linear part of the SAXS scattering curves acquired at different concentrations of magnesium (x-axis, in mM) for the catalytically incompetent variant A48-2′OCH_3 of the 2′−5′ AG1 lariat-forming ribozyme.

Role of Magnesium Ions. To further characterize the role of magnesium in supporting chemistry and folding in the 2′−5′ AG1 lariat-forming ribozyme, we used a two-step in silico protocol based on MD simulations in the Amber force field.[25] The first step consisted of predicting the magnesium binding sites in the structural model of the active state of the ribozyme. To this end, we equilibrated in two independent runs the model of the active fold of the 2′−5′ AG1 lariat-forming ribozyme in aqueous solution with K^+ ions corresponding to a concentration of 250 mM. After initial randomization of the ions positions, we monitored the sites where a K^+ ion was observed consistently for more than 50% of the simulation time. As demonstrated previously,[26] this protocol faithfully predicts the electronegative hot spots of RNA structures, which have been found to be occupied by Mg^{2+} ions in crystal structures. K^+ instead of Mg^{2+} ions are used in the in silico protocol for two reasons. First, the dehydration of Mg^{2+} ions occurs in the μs time scale. In the short time of the equilibration protocol (1.5 ns), the water molecules coordinating the magnesium cannot be substituted by the negatively charged functional groups in the inner coordination sphere. On the other hand, the dehydration of potassium ions occurs in less than 100 ps and can be efficiently achieved in the duration of the in silico protocol. Second, force field inaccuracies, related to the neglect of polarization and charge transfer effects, affect monovalent ions much less than divalent ions. For the 2′−5′ AG1 lariat-forming ribozyme, we find eight sites where a K^+ ion is consistently bound in both simulations.

In the next step of our in silico protocol, we substituted the K^+ ions at the conserved sites with Mg^{2+} ions, and we ran equilibration and energy minimization to optimize the geometry of their interaction with the RNA (Figure 6a). In this model, the G1-pro-$R_P\alpha$, the G1-pro-$S_P\beta$, and four water molecules coordinate one magnesium ion. In this position, the Mg^{2+} ion can dissipate the negative charge on the G1-phosphate, stabilize the penta-coordinated transition state, and stabilize the exiting diphosphate (Figure 6b). In addition, one of the coordinated water molecules forms a hydrogen bond with the G1-N7 (H−N distance, 2.4 Å, Figure 6c). This hydrogen bond increases the base character of the water molecule, which can extract the proton from the nearby A48-2′-O (O−O distance, 3.2 Å, Figure 6b) and initiate the reaction.

dx.doi.org/10.1021/ja311868t | J. Am. Chem. Soc. 2013, 135, 4403−4411

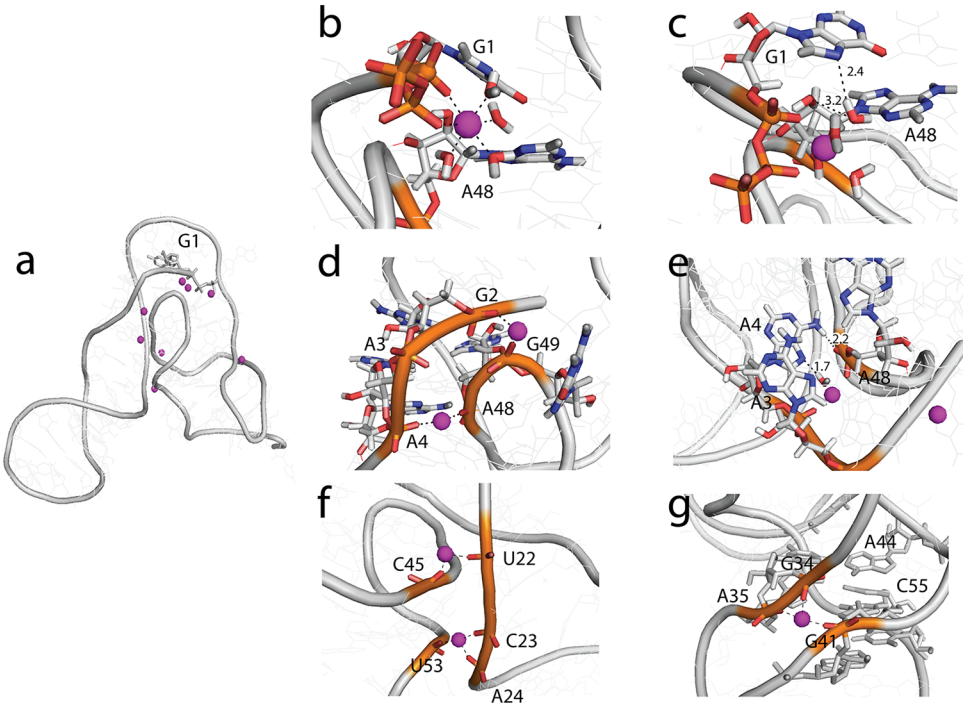

Figure 6. Position of the Mg^{2+} ions in the model of the active state of the 2′−5′ AG1 lariat-forming ribozyme. (a) Overview of the position of the magnesium ions. (b) The G1-pro-$R_P\alpha$, the G1-pro-$S_P\beta$, and four water molecules coordinate one magnesium ion at the catalytic site. A48 and G1 are shown in stick. C, H, gray, O, red, N, blue, P, orange. (c) A rotated view of panel a showing one of the Mg^{2+}-coordinating water molecule being involved in an hydrogen bond with the G1-N7 and at the same time being close to the A48-2′-O. Distances are in Å. (d) Two Mg^{2+} ions dissipate the negative charge concentration caused by the close proximity of the phosphate backbone of G2 and G49 and of A3-A4 and A48. G2-A4 and A48-G49 are shown in stick. (e) A rotated view of panel c showing the proximity of the exocyclic amino groups of A3-A4 to the phosphate of A48. A4-N7 and the A4-N6 participate in hydrogen bonds with a water molecule in the coordination sphere of one magnesium ion and the A48-pro-S_P, respectively. Distances are in Å. (f) Two Mg^{2+} ions stabilize the compact fold of the ribozyme by bridging the pro-R_P oxygens of U22, C23 and the pro-S_P oxygen of U53, and the pro-R_P oxygen of A24 and the pro-S_P oxygen of C45. Only the phosphates of the given nucleotides are shown. (g) One Mg^{2+} bridges the pro-R_P oxygen of G41 and the pro-S_P oxygen of G34, thereby stabilizing the stacking of H2 and H3.

The presence of this critical hydrogen bond involving the G1-N7 in the model is in very good agreement with the requirement of a purine at position 1. A second magnesium ion is coordinated by the G1-Pγ and further stabilizes the exiting diphosphate.

Third and fourth magnesium ions are coordinated by the phosphates of G2 and G49 and A4 and A48, respectively, thereby dissipating the concentration of negative charge at the contact points of the phosphate backbone of the C47-G49 stretch with that of the G1-A4 stretch (Figures 6d and 4c). The exocyclic amino groups of A3 and A4 are directed toward the phosphate of A48, further reducing the electrostatic repulsion (Figure 6e). In particular, A4-N7 and A4-N6 participate in hydrogen bonds with a magnesium-coordinating water molecule and the A48-pro-S_P, respectively, thereby providing a rationale for the need of an adenosine at position 4 (Figure 2). A fifth magnesium is close to the phosphate of C47.

Finally, in the model, two Mg^{2+} ions stabilize the compact fold of the ribozyme by bridging the pro-R_P oxygens of U22, C23 and the pro-S_P oxygen of U53, and the pro-R_P oxygen of A24 and the pro-S_P oxygen of C45, respectively (Figure 6f and 4c). An eighth Mg^{2+} stabilizes the stack of H2 and H3 by bridging the pro-R_P oxygen of G41, the pro-R_P oxygen of A35, and the pro-S_P oxygen of G34 (Figure 6g).

DISCUSSION

In this study we have used a combination of NMR spectroscopy, mutational analysis and computation to provide insight into the catalytic mechanism of the 2′−5′ AG1 lariat-forming ribozyme. We obtained the structure of the inactive state and a model of the active state of this self-reacting RNA. To our knowledge, this is the first atomic model of the active state of a lariat-forming ribozyme. Our data reveal that the position of the reaction center 5′-terminal guanosine is determined by a WC base pair between G1 and C27, which is part of a longer 5′-terminal helix; the major groove of the helix in proximity of the G1-C27 base pair appears to be significantly widened and likely accommodates parts of the RNA spanning the catalytic A48; we hypothesize that the catalytic A48 is specifically recognized by A26, which juxtaposes it onto the 5′-guanosine in a distance compatible with direct nucleophilic attack.

The secondary structure of the 2′−5′ AG1 lariat-forming ribozyme displays more base pairs than inferred from the co-variation.[7] The reason might lie in a too low sequence variability (20%) allowed in the selection procedure or in sequence bias introduced by the enzymes used in the protocol. Interestingly the region G1-A4 and A25-U28 was identified to be invariable in the SELEX experiment, in partial agreement with our finding, which indicate that the G1A/C27U double mutant is active as well. Similarly, in contrast to the SELEX results, we do not find that conservation of the stretches G32-A35 and A44-C47 is needed for activity, as long as the two stretches can form base pairs with each other (Figure 2).

The use of reduced model systems to infer the mechanisms of more complex enzymes has been a matter of debate for many

dx.doi.org/10.1021/ja311868t | J. Am. Chem. Soc. 2013, 135, 4403−4411

years.[27,28] Here, we wish to underline that no data are available validating that the catalytic mechanism of the 2′−5′ AG1 lariat-forming ribozyme is similar to that of the spliceosome or of introns II. Nevertheless, nature has evolved common pathways to perform a given task and it is reasonable to use the lesson learned from model systems to generate hypotheses. The validity of these hypotheses needs then to be tested for the more complex, native systems either in vitro or in vivo. Here, given the conservation of the attacking adenosine in lariat-forming ribozymes, we wonder if the recognition mode observed in the 2′−5′ AG1 lariat-forming ribozyme can be extended also to other catalytic RNAs and to the spliceosome. Strikingly, the spliceosome features a U downstream of the 5′ splice-site guanosine. This uridine could base pair with an adenosine and support the same mode of recognition for the catalytic adenosine as in the 2′−5′ AG1 lariat-forming ribozyme. In support of this, the G2U mutant, which converts the non-canonical G2·A26 base pair to a canonical one in the 2′−5′ lariat-forming ribozyme is catalytically competent, even if much less efficient than the wild-type ribozyme. For the role of the A26 equivalent adenosine in the spliceosome, a good candidate may be the fifth A of the conserved ACAGAGA box. In fact, cross-link between this A and the U next to the splice-site guanosine in the spliceosome has been previously reported.[29,30] In the spliceosome the catalytic adenosine is bulged out from a helical segment pairing the intron with the U2 RNA.[31] Similarly, in the 2′−5′ lariat-forming ribozyme the A48 is extruded from the pseudoknot structure at the tip of helix H2.

Interestingly, while the above ACAGAGA box is also present in the 2′−5′ lariat-forming ribozyme (nt's 29−35), our data indicate that it plays a different role than in the spliceosome. In the ribozyme the ACA sequence is not involved in any base pair, while the GAGA sequence has a critical structural role in the formation of the 3′ pseudoknot and in positioning the catalytic A48 close to the 5′ terminus. However, the ACAGAGA segment does not provide any functional groups to the chemical reaction, or Mg^{2+} binding.[7] In contrast, in the spliceosome the ACA segment was shown to base-pair with nucleotides close to the 5′ splice site, while the GAGA segment binds magnesium ions that are important for catalysis.[32,33]

In silico equilibration of the structural model of the active state of the 2′−5′ AG1 lariat-forming ribozyme in magnesium-containing buffer suggests that one magnesium ion is critical for chemistry. This Mg^{2+} is coordinated by the G1-N7 (through a water molecule) and the G1 α-phosphate (Figure 6b). The water molecule bridging between the Mg^{2+} and the G1-N7 is activated by the Mg^{2+} and the G1-N7 acting as bases and is in a favorable position to extract the A48-2′-O proton, thereby initiating catalysis. The position of the Mg^{2+} ion is compatible with the role of stabilizing the penta-coordinated phosphorus in the transition state and the exiting diphosphate. In support of this Mg^{2+} arrangement, the G1A/C27U double mutant, with a conserved purine at the 5′ terminus and the N7 available for Mg^{2+} coordination, is catalytically active, while the G1C/C27G mutant, which lacks the N7 on the 5′ terminus nucleotide, does not support chemistry. Interestingly, the same requirement for a purine residue at the 5′-terminal splice site is present also in the spliceosome, suggesting a conserved role for the N7 position of this nucleotide. However, in contrast to what proposed for the spliceosome and other ribozymes, which are thought to require two magnesium ions for catalysis,[34] the model of the active state of the 2′−5′ AG1 lariat-forming ribozyme predicts the involvement of only one Mg^{2+} at the reaction center. This conclusion has to be taken with caution, as the inaccuracy of the model of the active state of the 2′−5′ AG1 lariat-forming ribozyme, together with the limitation of the in silico modeling of ion binding sites, may be the cause for missing the second ion at the catalytic center.

In our model, other magnesium ions bind to the RNA phosphate backbone and stabilize the compact fold of the model of the active state of the ribozyme. The tight interaction of the major groove of the 5′-terminal helix with A48 brings the phosphate backbones of the 5′-terminal helix and the 3′-terminal pseudoknot in close proximity in the model. The electrostatic repulsion of the negatively charged RNA backbones is compensated by binding one magnesium ion at the phosphates of C45 and A24, one at the phosphates of U22, C23, and U53, and two at the phosphates of G2, A4, A48, and G49. In support of this model, phosphorothioate interference experiments have shown that binding of magnesium to the pro-R_P of G1-A3, C21, U22, A24, A25, and C47-G49 is essential for branching activity[7] (Figure 4c). Moreover, our SAXS data also show that the structure becomes more compact in the presence of magnesium. Taken together, magnesium ions are likely to have a double role in the 2′−5′ lariat-forming ribozyme: structural stabilization and involvement in the chemical reaction.

■ CONCLUSIONS

This study shows how integration of data from different disciplines can be combined to obtain structural models of states that are inaccessible to standard structural biology techniques. Mutational analysis data can be converted into an interaction network that, together with the structure of the accessible state of an enzyme, can be used in molecular modeling protocols to model the structure of other states. In the case of the 2′−5′ lariat-forming ribozyme, we were able to show that the branch-point adenosine may be recognized by an adenosine juxtaposed to the 5′-terminal nucleotide, one base pair downstream. The N7 atom of the 5′-terminal purine has been appointed a role in coordinating a magnesium ion, likely relevant to the activation of the attacking nucleophile. These findings allow us to draw parallels with the spliceosomal RNA and propose experiments to probe the role of the N7 atom of the guanosine at the 5′ splice site and the role of the fifth adenosine of the conserved ACAGAGA box in recognizing the branch-point adenosine in the first step of pre-mRNA splicing.

■ ASSOCIATED CONTENT

Supporting Information

Supplemental figures and tables referred to in the text, detailed experimental procedures, and pdb file for the model in Figure 4. This material is available free of charge via the Internet at http://pubs.acs.org.

■ AUTHOR INFORMATION

Corresponding Author

teresa.carlomagno@embl.de

Notes

The authors declare no competing financial interest.

■ ACKNOWLEDGMENTS

This work was supported by the EMBL, the MPG, and grant CA 294/2-1 from the DFG. We thank Frank Gabel for

discussion of the SAXS data and Claudia Schwiegk for precious help in sample preparation.

REFERENCES

(1) Will, C. L.; Lührmann, R. *Cold Spring Harbor Persp. Biol.* **2011**, *3*, a003707.
(2) Pyle, A. M.; Lambowitz, A. M. *The RNA World*, 3rd ed.; Cold Spring Harbor Laboratory Press: Cold Sping Harbor, NY, 2006.
(3) Cech, T. R. *Cell* **1986**, *44*, 207−210.
(4) Sharp, P. A. *Cell* **1985**, *42*, 397−400.
(5) Guthrie, C. *Science* **1991**, *253*, 157−163.
(6) Valadkhan, S.; Manley, J. L. *Nature* **2001**, *413*, 701−707.
(7) Tuschl, T.; Sharp, P. A.; Bartel, D. P. *RNA* **2001**, *7*, 29−43.
(8) Toor, N.; Keating, K. S.; Taylor, S. D.; Pyle, A. M. *Science* **2008**, *320*, 77−82.
(9) Chan, R. T.; Robart, A. R.; Rajashankar, K. R.; Pyle, A. M.; Toor, N. *Nat. Struct. Mol. Biol.* **2012**, *10*, 555−557.
(10) Tuschl, T.; Sharp, P.; Bartel, D. P. *EMBO J.* **1998**, *17*, 2637−2650.
(11) Hennig, M.; Williamson, J. R. *Nucleic Acids Res.* **2000**, *28*, 1585−1593.
(12) Dingley, A. J.; Grzesiek, S. *J. Am. Chem. Soc.* **1998**, *120*, 8293−8297.
(13) Sklenar, V.; Dieckmann, T.; Butcher, S. E.; Feigon, J. *J. Magn. Reson.* **1998**, *130*, 119−124.
(14) Hu, W. D.; Kakalis, L. T.; Jiang, L. C.; Jiang, F.; Ye, X. M.; Majumdar, A. *J. Biomol. NMR* **1998**, *12*, 559−564.
(15) Zwahlen, C.; Legault, P.; Vincent, S. J. F.; Greenblatt, J.; Konrat, R.; Kay, L. E. *J. Am. Chem. Soc.* **1997**, *119*, 6711−6721.
(16) Brünger, A. T.; Adams, P. D.; Clore, G. M.; DeLano, W. L.; Gros, P.; Grosse-Kunstleve, R. W.; Jiang, J. S.; Kuszewski, J.; Nilges, M.; Pannu, N. S.; Read, R. J.; Rice, L. M.; Simonson, T.; Warren, G. L. *Acta Crystallogr. Sect. D: Biol. Crystallogr.* **1998**, *54*, 905−921.
(17) Linge, J. P.; Habeck, M.; Rieping, W.; Nilges, M. *Bioinformatics* **2003**, *19*, 315−316.
(18) Ohlenschläger, O.; Haumann, S.; Ramachandran, R.; Görlach, M. *J. Biomol. NMR* **2008**, *42*, 139−142.
(19) Case, D. A.; Darden, T. A.; Cheatham III, T. E.; Simmerling, C. L.; Wang, J.; Duke, R. E.; Luo, R.; Walker, R. C.; Zhang, W.; Merz, K. M.; et al. *AMBER 11*; University of California, San Francisco, 2010.
(20) Jorgensen, W. L.; Chandrasekhar, J.; Madura, J. D.; Impey, R. W.; Klein, M. L. *J. Chem. Phys.* **1983**, *79*, 926.
(21) Hashem, Y.; Auffinger, P. *Methods (San Diego, Calif.)* **2009**, *47*, 187−197.
(22) Pernot, P.; Theveneau, P.; Giraud, T.; Fernandes, R. N.; Nurizzo, D.; Spruce, D.; Surr, J.; McSweeney, S.; Round, A.; Felisaz, F.; Foedinger, L.; Gobbo, A.; Huet, J.; Villard, C.; Cipriani, F. *J. Phys.: Conf. Ser.* **2010**, *247*, 12009.
(23) Konarev, P. V; Volkov, V. V; Sokolova, A. V; Koch, M. H. J.; Svergun, D. I. *J. Appl. Crystallogr.* **2003**, *36*, 1277−1282.
(24) Leontis, N. B.; Westhof, E. *Comp. Funct. Genom.* **2002**, *3*, 518−524.
(25) Pearlman, D. a.; Case, D. a.; Caldwell, J. W.; Ross, W. S.; Cheatham, T. E.; DeBolt, S.; Ferguson, D.; Seibel, G.; Kollman, P.; Cheatham Iii, T. E. *Comput. Phys. Commun.* **1995**, *91*, 1−41.
(26) Auffinger, P.; Bielecki, L.; Westhof, E. *Structure* **2004**, *12*, 379−388.
(27) Valadkhan, S.; Manley, J. L. *RNA* **2009**, *15*, 4−7.
(28) Smith, A. J.; Konarska, M. M. *RNA* **2009**, *15*, 1−3.
(29) Madhani, H. D.; Guthrie, C. *Annu. Rev. Genet.* **1994**, *28*, 1−26.
(30) Sontheimer, E. J.; Steiz, J. A. *Science* **1993**, *262*, 1989−1996.
(31) Parker, R.; Siciliano, P. G.; Guthrie, C. *Cell* **1987**, *49*, 229−239.
(32) Nilsen, T. W. In *RNA structure and function*; Simons, R. W., Grunberg-Manago, M., Eds.; Cold Spring Harbor Laboratory Press:: Cold Spring Harbor, NY, 1998; pp 303−357.
(33) Moore, M. J.; Query, C. C.; Sharp, P. A. In *The RNA world*; Gestland, R. F., Atkins, J. F., Eds.; Cold Spring Harbor Laboratory Press:: Cold Spring Harbor, NY, 1993; pp 303−357.
(34) Steiz, T. A.; Steiz, J. A. *Proc. Natl. Acad. Sci. U.S.A.* **1993**, *90*, 6498−6502.